



23rd International Conference on Material Forming (ESAFORM 2020)

## Capabilities of Macroscopic Forming Simulation for Large-Scale Forming Processes of Dry and Impregnated Textiles

Luise Kärger<sup>a,\*</sup>, Siegfried Galkin<sup>a</sup>, Dominik Dörr<sup>a,b</sup>, Christian Poppe<sup>a</sup>

<sup>a</sup>Karlsruhe Institute of Technology (KIT), Institute of Vehicle System Technology (FAST), Karlsruhe, Germany.

<sup>b</sup>SIMUTENCE GmbH, Karlsruhe, Germany.

\* Corresponding author. Tel.: +49-721 608-45386; E-mail address: [luise.kaerger@kit.edu](mailto:luise.kaerger@kit.edu)

### Abstract

Forming of continuously fibre-reinforced polymers (CoFRP) has a significant impact on the structural performance of composite components, underlining the importance of forming simulation for CoFRP product development processes. For an integrated development of industrial composite components, efficient forming simulation methods are in high demand. Application-oriented method development is particularly crucial for industrial needs, where large and complex multi-layer components are manufactured, commercial FE software is used, and yet high prediction accuracy is required. To meet industrial demands, this contribution gives an insight in macroscopic forming simulation approaches that utilize the FE software ABAQUS in combination with user-defined material models and finite elements. Three CoFRP forming technologies are considered, which are in industrial focus due to their suitability for mass production: textile forming of dry unidirectional non-crimp fabrics (UD-NCF), thermoforming of pre-impregnated UD tapes and wet compression moulding (WCM). In addition to the highly anisotropic, large-strain material behaviour that composite forming processes have in common, the three process technologies face various process-specific modelling challenges. UD-NCFs require material models that capture the deformation behaviour and the slippage of the stitching. Thermoforming of UD tapes is highly rate- and temperature-dependent, calling for rheological membrane and bending modelling. Moreover, a thermomechanical approach including crystallisation kinetics enables the prediction of potential phase-transition during forming and resulting defects in the semi-crystalline thermoplastic matrix. For simultaneous forming and infiltration in wet compression moulding, a finite Darcy-Progression-Element is superimposed with the membrane and shell elements for forming simulation, capturing infiltration-dependent material properties. The three outlined technologies illustrate the complexity and importance of further simulation method development to support future process development.

© 2020 The Authors. Published by Elsevier Ltd.

This is an open access article under the CC BY-NC-ND license (<https://creativecommons.org/licenses/by-nc-nd/4.0/>)

Peer-review under responsibility of the scientific committee of the 23rd International Conference on Material Forming.

*Keywords:* FE forming simulation; Large strain modelling; Forming effects; Draping; Non-crimp fabrics; thermoforming; wet compression moulding; ABAQUS

### 1. Introduction

For continuously fibre-reinforced plastics (CoFRP) components, the forming process is the decisive manufacturing step that forms the two-dimensional textile into three-dimensional shape. The resulting global and local forming effects have a significant impact on the structural performance and underline the importance of the forming process in the CoFRP product development process [1]-[2]. With the objective of an integrated product development of industrial composite components, efficient forming simulation methods

are required, firstly, to design the forming process and ensure defect-free formability, and secondly, to predict and transfer the resulting forming effects to subsequent simulation domains within a continuous CAE chain [3]. While great progress has been achieved in recent years to increase the accuracy of forming simulation methods, e.g. by local meso-modelling [4] or higher-order gradient approaches [5], application-oriented method development for efficient and yet reliable forming simulation is comparatively rare. This is particularly crucial for industrial needs, where large and complex multi-layer components are manufactured, commercial software is used,

2351-9789 © 2020 The Authors. Published by Elsevier Ltd.

This is an open access article under the CC BY-NC-ND license (<https://creativecommons.org/licenses/by-nc-nd/4.0/>)

Peer-review under responsibility of the scientific committee of the 23rd International Conference on Material Forming.

10.1016/j.promfg.2020.04.155

and yet high prediction accuracy is required to verify the formability and predict the final fibre architecture.

Efficient macroscopic CoFRP forming simulation can be divided in kinematic and constitutive approaches. Kinematic approaches are based on purely geometric mapping, while constitutive approaches take the material behaviour and process conditions into account. Although kinematic approaches neglect important physical mechanisms, they are often used for a rapid forming assessment in product development [6] or for applications in elaborate optimization loops [7]. However, kinematic forming simulation may severely deviate from reality [8], particularly for complexly curved geometries and multi-layer forming with case-specific process conditions. For such applications, macroscopic constitutive approaches are preferable. They are computationally more efficient than mesoscopic models and applicable for component forming simulation and virtual process design. Nevertheless, macroscopic models need to capture the relevant forming effects that occur on meso-scale and affect the macro-scale.

In this work, the basic modelling requirements and state of the art of macroscopic CoFRP forming simulation are outlined in Section 2. Subsequently, three macroscopic modelling approaches of large-scale CoFRP forming technologies are presented: textile forming simulation of stitched unidirectional non-crimp fabrics (UD-NCF, Section 3), thermoforming of pre-impregnated UD tapes (Section 4), and wet compression moulding (WCM, Section 5). These three process technologies imply material-specific modelling requirements, particularly in terms of mesoscopic effects due to stitching, thermomechanical effects including crystallisation kinetics, and superimposed infiltration during forming.

## 2. Basic deformation mechanisms and respective requirements for macroscopic forming simulation

### 2.1. Large shear and bending deformations

Macroscopic approaches describe the forming behaviour of textile products in a homogenised way, even though the textile does not represent a continuum on micro- and meso-scale. The multi-scale deformation behaviour is governed by the relative slip between the almost inextensible fibres. Due to this distinct fibre slippage, two main challenges arise for macroscopic material modelling. Firstly, the high tensile stiffness in fibre direction is combined with a very low shear stiffness, causing a high degree of anisotropy and large fibre rotations. Secondly, the high tensile stiffness is combined with a very low bending stiffness, which cannot be captured by conventional single-layer shell theories based on Cauchy mechanics.

The first requirement involves the correct modelling of large rotations of the principal material orientations and corresponding non-orthogonal strain and stress measures. Therefore, Green-Naghdi's frame, which is the orthogonal reference frame e.g. in the FE software ABAQUS, is not suitable to describe the deformation behaviour of fabrics [9]. Instead, geometrically non-linear constitutive models based on either hypoelastic or hyperelastic approaches need to be applied. In addition to the constitutive model, numerical shear or tension locking needs to be prevented either by the alignment of the FE

mesh to the fibre direction [10] or by a reduced integration with hour-glass stabilisation [11].

The second main requirement relates to the correct modelling of large fibre bending in conjunction with high tensile stiffness of the fibres. Classical single-layer shell theories based on Cauchy mechanics are not capable to capture this behaviour [5]. Reproducing out-of-plane bending with classical Cauchy continuum mechanics requires a decoupling of membrane and bending behaviour. In application-oriented forming simulation, this is typically achieved by superimposing conventional membrane and plate elements [12]-[14]. Alternatively, a DKT shell element formulation with integrated decoupled constitutive equations for membrane and bending is applied [15]. As an efficient combination of mesoscopic features with macroscopic modelling, semi-discrete shell elements are proposed, utilizing a quasi-mesoscopic decomposition of the deformation mechanisms of tension, shear and bending [16]-[17]. A purely continuous mechanical framework without decoupling of membrane and bending can be achieved by second gradient continuum approaches [5], [18]. In this way, fibre bending is taken into account independently of the first gradient behaviour. Such a generalized continuum formulation captures not only out-of-plane, but also in-plane fibre bending. In application-oriented Cauchy continuum approaches, on the contrary, in-plane fibre bending is typically ignored or is captured in a simplified smeared way by in-plane shear.

### 2.2. Hypo- and hyperelastic modelling in application-oriented macroscopic FE forming simulation

To account for large fibre rotations and non-orthogonal principal material orientations in macroscopic forming simulation, geometrically non-linear constitutive models based on either hypoelastic or hyperelastic approaches are applied. The advantage of hypoelastic approaches is their comparatively easy implementation in commercial FE software. However, hypoelastic approaches are path-dependent due to their rate-related formulation, and thus, require sufficiently small integration step widths to achieve sufficiently accurate results.

In the FE software ABAQUS, the hypoelastic *\*Fabric* material model is available to describe the deformation behaviour of materials with non-orthogonal material frame by characteristic curves for shear and fibre-tension behaviour. The model is widely used in industrial applications for forming simulation of woven textiles. However, an interaction between tensile and shear properties, non-orthogonal bending and non-orthogonal Poisson's contraction cannot be captured by this model [14]. For that purpose, user-defined material subroutines (V)UMAT are needed, as proposed for forming simulation with ABAQUS for hypoelastic modelling of UD-NCF [14], of woven fabrics [19] and thermoplastic woven tapes [20].

To utilize the advantages of hyperelastic modelling, Dörr et al. [13] developed a combined hyper-hypoelastic approach to perform forming simulation of UD tapes using Abaqus built-in finite elements. This combination is needed, since the preferable hyperelasticity can only be implemented for the membrane behaviour with ABAQUS built-in finite membrane elements. To model bending behaviour, a user-defined shell

section integration in a so-called (V)UGENS subroutine is needed [13]. In contrast to a (V)UMAT, a (V)UGENS does not allow for implementing hyperelastic equations, since only the incremental curvature change is available in ABAQUS, not the absolute surface gradient. Therefore, hypoelastic modelling is required for bending. Since forming simulation usually applies an explicit time integration, time steps are typically small, causing a negligible numerical error in hypoelastic modelling. For pure hyperelastic forming simulation, however, user-defined finite shell elements need to be implemented in ABAQUS. Therefore, Dörr et al. [15] implemented a shell element based on Discrete Kirchhoff Theory (DKT), where the virtual internal energy  $\delta W^{\text{in}}$  is decomposed into a membrane and a bending part,

$$\delta W^{\text{in}} = \int_V [S_{\alpha\beta}^{\text{mem}} \delta E_{\alpha\beta} + S_{\alpha\beta}^{\text{bend}} \delta E_{\alpha\beta}] dV \quad (1)$$

with the Green-Lagrange strain  $E_{\alpha\beta}$  and the second Piola-Kirchhoff (PK2) stress  $S_{\alpha\beta}$ .

### 2.3. Material-specific deformation mechanisms

In addition to large shear and bending deformations, further requirements for macroscopic modelling originate from the structural characteristics of individual textile materials. This textile architecture strongly influences the deformation behaviour, and material models must capture the specific deformation mechanisms. Two main types are distinguished: dry engineering textiles and pre-impregnated textiles, which are also called tapes in the case of thermoplastic matrices.

*Dry engineering textiles* typically used for shell-like components are woven fabrics and non-crimp fabrics (NCF). NCFs provide a higher lightweight potential than woven fabrics due to their straight fibres without undulations. Among NCFs, unidirectional (UD) NCFs enable a more targeted tailoring than biaxial NCFs, since one fabric layer contains only one fibre direction. Thus, UD-NCFs provide the highest lightweight potential among the dry textile's family. However, their formability is much more challenging in comparison to bidirectional fabrics. The better formability of woven fabrics for complex geometries is the main reason that the majority of research work on textile forming addresses woven fabrics [19], [21][22]. In contrast, forming of Biaxial-NCF [23]-[24] or even UD-NCF [3], [14], [25], [26] has been investigated much less. However, since the lightweight potential of UD-NCF is increasingly attractive also for complexly curved components in automotive and aerospace applications, there is an increasing demand for research on forming of UD-NCF, which is therefore addressed in this review. While *woven fabrics* are intrinsically cohesive due to the interwoven fibre yarns, the yarns of *non-crimp fabrics (NCF)* are bonded together by a stitching pattern. Due to the trellis effect of woven fabrics, their intrinsic deformation mode is pure shear. In contrast, shear strain of UD-NCF is superimposed by transverse tensile strain, which may be substantial [25]-[26]. Macroscopic material models need to capture this superposed membrane behaviour in a suitable way. Off-axis-tension (OAT) tests have been performed to investigate the multiaxial deformation behaviour and to serve for membrane model development [14]. The low transverse stiffness highly depends on the type of stitching and on the

slippage between stitching and fibre yarns. The resulting transverse tensile deformation leads to gapping between the fibre yarns. Furthermore, depending on the lateral contraction of the stitching, mesoscopic buckling of the fibre yarns may occur [26].

The deformation behaviour of *pre-impregnated textiles* (e.g. woven and UD thermoplastic tapes) differs from dry textiles mainly by the distinct rate- and temperature-dependency [27]. In the case of woven tapes, the basic deformation mechanism is pure shear, as for woven fabrics, but combined with a pronounced viscoelasticity [28]. In the case of UD tapes, superimposed shear and transverse tension occurs, as for UD-NCF. This combined shear and transverse tension is controlled by the isotropic viscoelastic matrix, which can be superimposed to the UD fibre stiffness [27], [29]. In this regard, it is easier to characterize and model the deformation behaviour of impregnated UD tapes compared to the complex deformation and slipping behaviour of the stitching in UD-NCF.

## 3. Macroscopic forming simulation of stitched UD-NCF

### 3.1. Hypoelastic-plastic modelling of UD-NCF

According to the deformation mechanisms described in Section 2.3, membrane modelling of UD-NCF needs to capture large shear strains  $\gamma_{12}$  superimposed with large non-orthogonal transverse tensile strains  $\varepsilon_2$  and perpendicular compressive strains  $\varepsilon_1$ , cf. Fig. 1(a). In case of large shear strains  $\gamma_{12}$ , tensile strains  $\varepsilon_2$  and compressive strains  $\varepsilon_1$  may occur simultaneously, resulting in transverse compaction [14]. In contrast, gapping occurs only in case of large tensile strain  $\varepsilon_2$  at moderate shear strain  $\gamma_{12}$ .

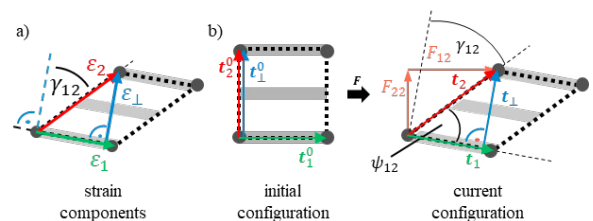


Fig. 1. (a) Transverse strain  $\varepsilon_2$  versus perpendicular strain  $\varepsilon_1$ ; (b) deformation of line segments  $\mathbf{t}_1$ ,  $\mathbf{t}_2$  and  $\mathbf{t}_1$ , based on [14].

Modelling large shear deformation requires suitable non-orthogonal strain and stress measures. For UD-NCF, Schirmaier et al. [14] proposed an alternative formulation of the strain measures. Two line segments  $\mathbf{t}_i^0$  represent the material's principal directions in the initial configuration. Line segment  $\mathbf{t}_1^0$  corresponds to the fibre direction, while line segment  $\mathbf{t}_2^0$  corresponds to the direction of the stitching, cf. Fig. 1(b). After deformation, the linear but non-orthogonal strain components  $\varepsilon_1$  of the fibres and  $\varepsilon_2$  of the stitching are defined by

$$\varepsilon_i = \frac{|\mathbf{t}_i|}{|\mathbf{t}_i^0|} - 1 = \sqrt{\sum_j F_{ji}^2} - 1, \quad j = 1, 2 \quad (2)$$

where the line segments  $\mathbf{t}_i = \mathbf{F} \cdot \mathbf{t}_i^0$  of the current configuration result from the deformation gradient  $\mathbf{F}$ . The shear angle  $\gamma_{12}$  is calculated from the relative orientation of the line segments  $\mathbf{t}_i$ .

$$\gamma_{12} = \frac{\pi}{2} - \psi_{12} = \frac{\pi}{2} - \cos^{-1} \left( \frac{\mathbf{t}_1 \cdot \mathbf{t}_2}{|\mathbf{t}_1| |\mathbf{t}_2|} \right) \quad (3)$$

Additionally, the linear perpendicular strain component  $\varepsilon_{\perp}$  is introduced based on the line segment  $\mathbf{t}_{\perp}$  perpendicular to  $\mathbf{t}_1$ :

$$\begin{aligned} \varepsilon_{\perp} &= \frac{|\mathbf{t}_{\perp}|}{|\mathbf{t}_1^0|} - 1 = \frac{|\mathbf{t}_2| \sin(\psi_{12})}{|\mathbf{t}_2^0|} - 1 \\ &= \sqrt{F_{12}^2 + F_{22}^2} \sin(\psi_{12}) - 1 \end{aligned} \quad (4)$$

cf. Fig. 1(a) [14].

Corresponding to the non-orthogonal linear strain components  $\varepsilon_1, \varepsilon_2, \gamma_{12}$ , the nominal stress tensor  $\mathbf{P}^*$  can be formulated based on an orthogonal material stiffness matrix by

$$\mathbf{P}^* = \begin{pmatrix} P_{11}^* \\ P_{22}^* \\ P_{21}^* \end{pmatrix} = \begin{pmatrix} \frac{E_1}{1 - \nu_{12}\nu_{21}} & \frac{\nu_{21}E_1}{1 - \nu_{12}\nu_{21}} & 0 \\ \frac{\nu_{12}E_2}{1 - \nu_{12}\nu_{21}} & \frac{E_2}{1 - \nu_{12}\nu_{21}} & 0 \\ 0 & 0 & G_{12} \end{pmatrix} \begin{pmatrix} \varepsilon_1 \\ \varepsilon_2 \\ \gamma_{12} \end{pmatrix} \quad (5)$$

accounting for large shear strains. In addition to the linear elastic non-orthogonal material behaviour, a non-linear elastic-plastic formulation is introduced by Schirmaier et al. [14]. In this material model, the total tensile strain  $\varepsilon_2$  and the total shear angle  $\gamma_{12}$  are composed of elastic as well as hardening plastic parts. A yield condition defines the transition from elastic to plastic domain.

In contrast to the tensile stress  $P_{22}^*$  of the stitching, transverse compression can only be transmitted perpendicular to the carbon fibres. This compressive stress  $P_{\perp}$  is modelled via an additional nonlinear elastic material law depending on  $\varepsilon_{\perp}$  and  $\gamma_{12}$  [14]. The perpendicular compressive strain  $\varepsilon_{\perp}$  may occur together with the transverse tensile strain  $\varepsilon_2$ , cf. Fig. 1(a). In case both strain components have equal sign, disjunction between the two stresses needs to be ensured. Therefore, the transverse stress  $P_{22}^*$  is set to zero for  $\varepsilon_2 < 0$  and the perpendicular stress  $P_{\perp}$  is set to zero for  $\varepsilon_{\perp} > 0$ . A more detailed description of the hypoelastic-plastic UD-NCF membrane model is given in [14]. The model parameters for shear and transverse tension have been identified based on experimental off-axis tension (OAT) tests of UD-NCF with three different fibre orientations  $\theta = \{30^\circ, 45^\circ, 60^\circ\}$  [14], [30].

### 3.2. Macroscopic forming simulation and prediction of forming effects in stitched UD-NCF

Based on the modelling approach for UD-NCF, the fibre orientation of the current configuration  $\mathbf{t}_1 = \mathbf{F} \cdot \mathbf{t}_1^0$  is computed by the initial fibre orientations  $\mathbf{t}_1^0$  and the deformation gradient  $\mathbf{F}$ . The shear angle  $\gamma_{12}$  is given in Eq. (3). The fibre volume content (FVC) yields

$$\varphi_f = \frac{A}{A_0} \varphi_{f0} \quad (6)$$

depending on the initial FVC  $\varphi_{f0}$  and the ratio between the initial area  $A_0$  and the deformed area

$$A = \det(\mathbf{F}) A_0 = (F_{11}F_{22} - F_{12}F_{21}) A_0 \quad (7)$$

In addition to fibre orientation, shear angle and FVC, the modelling approach of Section 3.1 provides indication to analyse three further forming effects: gapping, transverse

compaction and fibre waviness [30]. Gaping and transverse compaction result from the perpendicular strain component  $\varepsilon_{\perp}$ , where gaping corresponds to tensile strains and compaction to compressive strains. Fibre waviness may occur at meso scale in the form of undulations with an amplitude to wavelength ratio  $A_{\lambda}/\lambda$ . Such undulations cannot be captured macroscopically and are expected to arise in regions with compressive fibre strain,  $\varepsilon_1 < 0$ , due to fibre buckling. Hence, ratio  $A_{\lambda}/\lambda$  can be deduced from  $\varepsilon_1$ , but depends on the compressive stiffness in fibre direction, which impedes a quantitative evaluation. For varying process conditions, however, a qualitative evaluation and comparison of the susceptibility to waviness is facilitated.

The UD-NCF modelling approach is applied to a three-dimensionally curved L-shaped geometry, illustrated in Fig. 2. Experimental forming tests on this geometry have been performed at ILK Dresden [31]. A first comparison between simulation and experimental results is shown in Fig. 2c, which indicates a good agreement of the overall deformation state and of the outer contour of the formed textile. Furthermore, local forming effects are evaluated. The UD-NCF modelling approach enables a detailed analysis of forming effects for various layups and process condition. Fig. 3 shows exemplary results (fibre volume content, fibre waviness, gaping and transverse compaction) for the  $90^\circ$  layer in a  $0^\circ/90^\circ$  layup of UD-NCF. Two process conditions are compared: free forming without blank holders and constrained forming with 20 blank holders of 250 N each, continuously distributed around the L-shape. The simulation results demonstrate the influence of process conditions on local forming effects: The fibre volume content and the tendency to fibre waviness are reduced due to the blank holder forces, particularly at the curved right edge of the L-profile, where the forming travel is the largest. Consequently, gaping between the fibres is increased in these regions (Fig. 3b). In both process scenarios, transverse compaction is small within the inner region and large beyond the outer edges, particularly near the corners. Due to the high shear strains outside the corners, compressive strains occur perpendicular to the fibres and macroscopic wrinkles arise parallel to the fibres. This effect is slightly reduced by activating the blank holders. To optimize the influence of the blank holders, forming simulation can be used for process design, as shown before for clamping strategies to form woven fabrics [1].

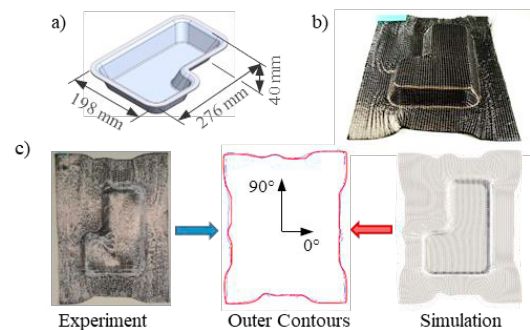


Fig. 2. (a) L-shaped geometry [31]. (b) Preform of a UD-NCF [31]. (c) Experimental (blue) and numerical (red) forming results of a  $90^\circ$  layer in a  $0^\circ/90^\circ$  layup of UD-NCF: Deformation state and outer contours.

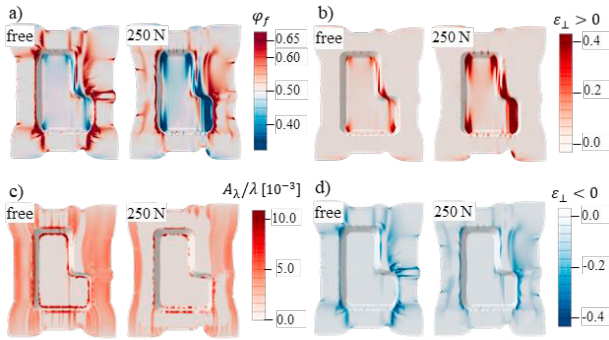


Fig. 3. Forming simulation results in the 90° layer of a 0°/90° UD-NCF layup formed without blank holders (free) and with 250N blank holders. Forming effects: (a) fibre volume content  $\phi_f$ , (b) gaping  $\varepsilon_{\perp} > 0$ , (c) fibre waviness  $A_{\lambda}/\lambda$ , and (d) transverse compaction  $\varepsilon_{\perp} < 0$ .

For comparison with experimental results, the local forming effects have been analysed manually at ILK Dresden [31]. The extent of gaping was determined by measuring the roving distance in critical areas. The critical areas are plotted by accordingly coloured ellipses. Fig. 4 exemplarily shows the amount of gaping within the 90° layer of a 0°/90° UD-NCF layup. A reasonable agreement is observed for the distribution of gaping and its concentration in the corner areas. However, the extent of gaping is overestimated by simulation. The deviation can be traced back to the macroscopic approach, which captures gaping in a homogeneous way and relates it directly to the perpendicular tensile strain  $\varepsilon_{\perp}$ . Distinct mesoscopic effects are not modelled, but may occur, for example, due to different contact conditions of fibre yarns and stitching to adjacent layers, particularly at geometrical edges. These locally varying boundary conditions contradict the homogeneous description. Furthermore, gaping is less pronounced, if fibre yarns are continuously spread rather than distinctively taken apart from each other. This local effect is ignored and limits the capability of macroscopic forming simulation to predict local forming effects. Nevertheless, the resulting strain fields of macroscopic approaches are valuable measures for virtual process design, e.g. for numerical evaluation of different UD-NCF layups and process conditions.

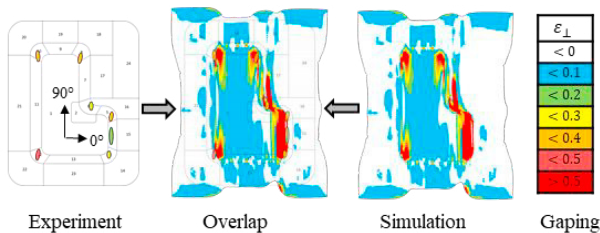


Fig. 4. Comparison of experimentally and numerically determined gaping in the 90° layer of a 0°/90° UD-NCF preform, formed with 250 N blank holders.

## 4. Coupled thermomechanical forming simulation

### 4.1. Thermo-hyperviscoelastic modelling of UD tapes

As outlined in Section 2.3, pre-impregnated textile materials show a pronounced rate-dependent deformation behaviour, which requires suitable rheological models. To model the rate-dependent shear behaviour of pre-impregnated woven tapes, several authors present nonlinear hyper- and hypoviscoelastic models based on a Voigt-Kelvin or a generalized Maxwell approach [12], [20], [32]. For UD tapes, Dörr et al. [15] proposed nonlinear hyperviscoelastic models based on Voigt-Kelvin and Generalized Maxwell approaches, implemented in a user-defined "Discrete Kirchhoff Theory" (DKT) shell formulation in ABAQUS.

The rate-dependent bending behaviour of pre-impregnated textiles is often neglected by thermoforming simulation approaches [12], [32]. However, a pronounced rate-dependency is observed in rheometer bending tests. Moreover, it has been shown that it is crucial for accurate prediction of wrinkling [13]. Therefore, Dörr et al. [13] modelled rate-dependent bending of UD tapes based on a Voigt-Kelvin and a generalized Maxwell approach, and demonstrated the impact on wrinkling behaviour at component-level.

For a coupled thermomechanical analysis of the thermoforming of UD tapes, the hyperviscoelastic membrane and bending models in [13], [15] are adopted and enhanced for thermal behaviour as well as temperature- and crystallization-dependent mechanical behaviour [33]. By this coupled thermomechanical extension, a numerical process evaluation in terms of non-isothermal effects, early crystallisation and process-dependent wrinkling becomes possible. A smooth phase transition between molten and solid material state is modelled by formulating the constitutive equations for both material states and superimposing the resulting second Piola Kirchhoff (PK2) stress tensors for the molten state  $S^m$  and the solid state  $S^s$ :

$$S = (1 - X) S^m + X S^s \quad (8)$$

utilizing the relative crystallinity  $X$  [38]. A multiplicative decomposition of the deformation gradient  $F = F^s \cdot F^m$  into a solid and a molten part is applied, where the intermediate configuration  $F^m$  represents the onset of crystallization. Accordingly, the Green-Lagrange strain in the initial configuration splits additively into  $E = E^s + E^m$ .

Viscoelastic constitutive equations according to [13], [15] are applied to model the molten material state: The membrane behaviour is modelled based on the "Ideal Fibre-Reinforced Material" (IFRM) model [34], where a linear-elastic uniaxial fibre model is superimposed with an isotropic hyperviscoelastic model for the matrix. Additionally, an anisotropic hyperviscoelastic constitutive equation is applied for bending. For the solid state, the hyperelastic St. Venant-Kirchhoff model is applied,  $S^s = C E^s$ , where the fourth order elasticity tensor  $C$  represents the orthotropic material behaviour. The thermal behaviour during thermoforming is modelled based on the heat balance equation, including internal heat conduction, heat loss at the tool-ply interfaces and convection and radiation at the free laminate surfaces. Moreover, crystallization kinetics as well as related latent heat

generation is modelled based on the approach by Ziabicki [35] and following the enhancement for several cooling rates [36]. The model parameters for the viscoelastic membrane and bending behaviour are determined by rheometer torsion bar tests and rheometer bending tests, respectively [15]. For thermal behaviour, standard and fast differential scanning calorimetry (S-DSC, F-DSC) measurements are conducted to characterize heat capacity and crystallization kinetics at moderate and high cooling rates [33]. For convection, radiation and tool-ply conductance, cooling experiments have been performed [37].

#### 4.2. Thermoforming process evaluation by coupled thermomechanical simulation of UD tapes

The thermomechanical modelling approach presented by Dörr et al. [33] and shortly outlined above has been applied to thermoforming simulation of a complexly shaped geometry. The simulation results have been validated by experimental tests with orthotropic and quasi-isotropic layups [33]. Fig. 5 illustrates the results of the quasi-isotropic layup. In addition to the thermomechanical approach, an isothermal approach is applied, assuming a constant temperature of 270 °C, which is slightly below the pre-heated layup temperature of 285 °C. While the isothermal approach clearly underestimates the wrinkling behaviour, the thermomechanical approach reflects the wrinkling better. Moreover, the outer contour of the blank is predicted with a better agreement by the thermomechanical approach than with the isothermal approach, particularly at the top side. The improved accuracy is attributable mainly to the consideration of the local cooling at tool-ply contact. The locally reduced temperature is illustrated in Fig. 5d, while Fig. 5e shows the cooling rate. Consequently, the relative crystallinity is highest at regions with low temperature. The isothermal approach does account neither for temperature-dependent properties nor for the beginning crystallization and crystallinity-dependent material behaviour [33].

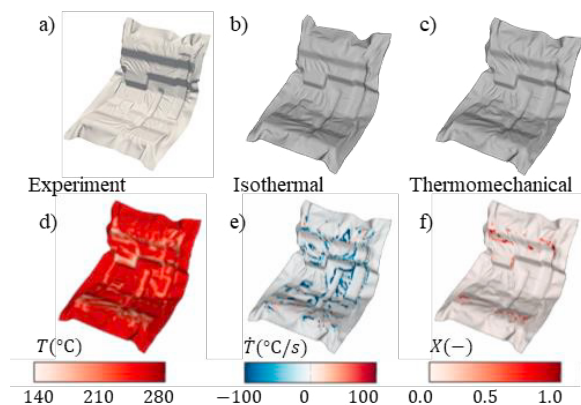


Fig. 5. Thermoforming of a quasi-isotropic layup [0, -45, 90, 45], at a remaining tool travel of 5mm and a tool temperature of 110 °C: Comparison between (a) experimental tests, (b) isothermal simulation ( $T = 270$  °C), and (c) thermomechanical simulation, according to [33]. Thermomechanical simulation results of the lowest ply: (d) temperature, (e) rate of temperature, and (f) relative crystallinity [38].

The coupled approach enables a numerical analysis of varying process parameters and their impact on the thermoforming behaviour. For that purpose, Dörr [38] varied the process parameters tool temperature and forming velocity in thermoforming simulation. It could be shown that both parameters have a considerable influence on the local temperature and on crystallization, as exemplarily shown in Fig. 6 for varying forming velocities at constant tool temperature of 110 °C. For low forming velocities, the temperature drops further and extensive crystallization occurs during forming, leading to more wrinkling. In contrast, a higher forming velocity yields less wrinkling. The same tendency is found for low tool temperatures (70 °C) compared to high tool temperatures (150 °C) and could be confirmed by experimental tests [38]. In a qualitative comparison, the predicted wrinkling behaviour and sensitivities are in good agreement with the experimental one. Some deviations are identified in terms of the sensitivity to tool temperature, which is slightly underestimated by the thermomechanical approach. This deviation is probably caused by underestimated tool-ply conductance. It might be induced either by uncertainty in the measured tool-ply gap conductance or by limited model refinement at regions of tool-ply interaction.

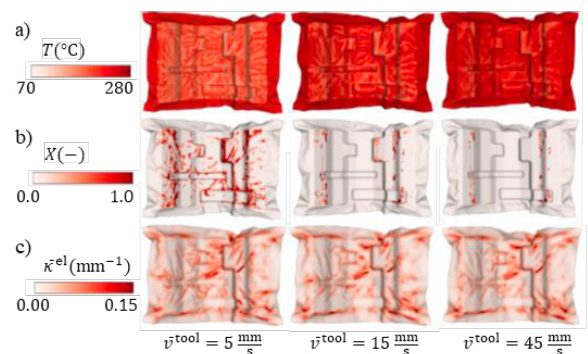


Fig. 6. Thermoforming of a quasi-isotropic layup [0, -45, 90, 45], at a remaining tool travel of 5mm and a tool temperature of 110 °C: Comparison of (a) temperature, (b) relative crystallinity, and (c) mean curvature (representing wrinkling) for three mean forming velocities [38].

Overall, the thermomechanical thermoforming simulation approach is capable to take relevant process parameters and material characteristics into account, including the phase transition from molten to solid state. Therewith, the prediction accuracy of thermoforming simulation has been distinctively improved, providing a valuable step towards reliable virtual process analysis and virtual process design.

## 5. Coupled forming and injection modelling for wet compression moulding

As a promising alternative to resin transfer moulding (RTM) of dry textiles, wet compression moulding (WCM) provides a high potential for large-scale production of CoFRP components [39]. Due to simultaneous forming and infiltration, low cycle times can be achieved and low cavity pressures are sufficient, making the process attractive for industrial applications. Up to

now, decisive process parameters such as internal cavity pressure, fibre displacements (fibre washing), optimum mould closing profiles, or sealing concepts cannot be predicted virtually. For reliable simulation of WCM processes, a coupled approach of textile deformation and resin propagation is required [40]. This includes three modelling domains: Firstly, forming simulation including infiltration-dependent viscoelastic material modelling (viscous draping), secondly, a solution of the fluid pressure field under consideration of the current deformation state (simultaneous infiltration), and thirdly, a coupling between fluid pressure and textile deformation (fluid-structure-interaction), cf. Fig. 7.

Macroscopic CoFRP forming approaches, as outlined for dry and pre-impregnated UD textiles in Sections 3 and 4, can be adapted to model the first modelling domain, the viscous draping behaviour in WCM. Therefore, experimental studies have been performed to investigate the infiltration- and rate-dependent deformation behaviour of woven fabrics in shear [41], bending [42] and inter-ply contact [43]. Based on the experimental results, infiltration-dependent constitutive equations are parametrized and implemented in the forming simulation framework. Numerical studies on component level demonstrate the sensitivity of the infiltration-dependent mechanical properties on the overall forming behaviour, particularly on the formation of wrinkles [41]-[43].

To model simultaneous resin propagation, a two-dimensional mould-filling approach based on Darcy's law has been implemented and verified within the forming simulation framework [40]. Beyond the determination of the pressure distribution in the saturated domain, the flow front propagation needs to ensure mass conservation

$$\dot{V} = \int_V \operatorname{div} \left( \operatorname{grad} \left( \frac{\mathbf{K}}{\eta * \phi} p \right) \right) dV \rightarrow 0 \quad (9)$$

where  $\dot{V}$  is the fluid volume rate within the saturated domain  $V$ ,  $\mathbf{K}$  the permeability tensor,  $\eta$  the fluid viscosity,  $\phi$  the fibre volume content and  $p$  the fluid pressure. To ensure mass conservation, a transient global control volume (CV) is implemented, considering the summation of the volume flow at the outer edges (inlet, flow front, wall, outlet). To model the combined WCM process, the 2D mould-filling approach is superposed by the viscous draping approach described above. The transient local fibre orientations resulting from the draping approach are directly coupled to the fluid propagation via the local fibre-parallel permeability tensor  $\mathbf{K}$  in Darcy's law. Vice versa, the presence and the transient viscosity of the resin, resulting from the mould-filling approach, directly influences the deformation behaviour and, thus, the material model parameters of the dry or infiltrated textile.

Current research aims to extend the two-dimensional approach to a fully three-dimensional model which is required to suitably represented the WCM process boundary conditions and the 3D fluid progression [44]. Additionally, an extension of the applied draping model with respect to material compaction in thickness direction is required [45]. In future work, 3D modelling and FSI is particularly important in order to describe the last phase of the tool closure, where fluid pressure is comparatively high and global forming occurs primarily in thickness direction.

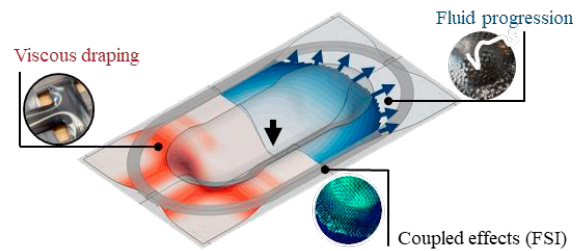


Fig. 7. Simultaneous forming and infiltration during Wet Compression Moulding of a double dome geometry, according to [43].

## 6. Conclusions and future trends

With the objective of an efficient process design for large-scale production, this contribution presents macroscopic FE forming simulation methods that are appropriate for industrial applications. Three forming technologies are currently in industrial focus due to their suitability for mass production: textile forming of dry unidirectional non-crimp fabrics (UD-NCF), thermoforming of pre-impregnated UD tapes and wet compression moulding (WCM). The presented macroscopic approach for stitched UD-NCF captures the global deformation behaviour very well, but lacks prediction accuracy in terms of local effects like gaping between fibre yarns. Therefore, future research will focus on more accurate, but still efficient modelling of mesoscopic effects, e.g. the slippage between stitching and fibre yarns. For this purpose, higher order gradient approaches might be a promising strategy.

The forming simulation approach presented for thermoplastic UD tapes includes rate- and temperature-dependent hyperviscoelastic material modelling as well as thermal modelling and crystallisation kinetics. It supports the prediction of early transition from molten to solid phase and the influence on forming results like wrinkling and matrix failure. It thus provides a valuable tool for virtual process design.

For simultaneous forming and infiltration in wet compression moulding, a two-dimensional approach based on Darcy's law and infiltration-dependent intra- and inter-ply properties has been presented. An enhancement towards a fully coupled 3D simulation approach is aspired to capture 3D fluid progression, 3D textile forming and potential fibre washing.

## Acknowledgements

The authors are grateful for the financial support of the research projects that led to the presented results: the Young Investigator Group (YIG) "Green Mobility", funded by the Vector Foundation, the DFG project "Experimental and virtual analysis of draping effects" (KA4224/1-1), the BMBF project SMiLE, and the project "Forschungsbrücke", funded by the State Ministry of Baden-Württemberg. The authors would also like to thank ILK Dresden for the experimental draping tests of UD-NCF, and Fraunhofer ICT for the experimental thermoforming and wet compression moulding tests used for validation.

## References

- [1] Kärger L, Galkin S, Zimmerling C, Dörr D, Linden J, Oeckerath A, Wolf K: Forming optimisation embedded in a CAE chain to assess and enhance the structural performance of composite components. *Compos Struct* 192: 143-152, 2018.
- [2] Henning F, Kärger L, Dörr D, Schirmaier FJ, Seuffert J, Bernath A: Fast processing and continuous simulation of automotive structural composite components. *Compos Sci Techn* 171: 261-279, 2019.
- [3] Kärger L, Bernath A, Fritz F, Galkin S, Magagnato D, Oeckerath A, Schön A, Henning F: Development and validation of a CAE chain for UD fibre reinforced composite components. *Compos Struct* 132: 350–358, 2015.
- [4] Iwata A, Inoue T, Naouar N, Boisse P, Lomov SV: Coupled meso-macro simulation of woven fabric local deformation during draping. *Compos A* 118: 267-280, 2019.
- [5] Boisse P, Bai R, Colmars J, Hamila N, Liang B, Madeo A: The need to use generalized continuum mechanics to model 3d textile composite forming. *Applied Composite Materials* 25(4):761–771, 2018.
- [6] Pickett AK, Creech G, de Luca P (2005). Simplified and advanced simulation methods for prediction of fabric draping. *Revue Européenne des Éléments Finis*, 14(6-7):677–691.
- [7] Fengler B, Kärger L, Henning F, Hrymak A. Multi-objective patch optimization with integrated kinematic draping simulation for continuous–discontinuous fiber-reinforced composite structures. *J Compos Sci* 2(2):22, 2018.
- [8] Vanclooster K, Lomov SV, Verpoest I. Experimental validation of forming simulations of fabric reinforced polymers using an unsymmetrical mould configuration. *Comp A* 40(4):530–539, 2009.
- [9] Badel P, Vidal-Sallé E, Boisse P. Large deformation analysis of fibrous materials using rate constitutive equations. *Computers & Structures*, 86(11–12):1164–1175, 2008.
- [10] Yu X, Cartwright B, McGuckin D, Ye L, Mai YW. Intra-ply shear locking in finite element analyses of woven fabric forming processes. *Compos A* 37(5):790–803, 2006.
- [11] Hamila N, Boisse P. Locking in simulation of composite reinforcement deformations. analysis and treatment. *Compos A* 53:109–117, 2013.
- [12] Haanappel SP, ten Thije R, Sachs U, Rietman B, Akkerman R. Formability analyses of uni-directional and textile reinforced thermoplastics. *Compos Part A: Appl Sci Manuf*;56:80–92, 2014.
- [13] Dörr D, Schirmaier F, Henning F, Kärger L: A viscoelastic approach for modeling bending behavior in FE forming simulation of continuously fiber reinforced composites. *Compos A* 94: 113-123, 2017.
- [14] Schirmaier FJ, Dörr D, Henning F, Kärger L: A macroscopic approach to simulate the forming behaviour of stitched unidirectional non-crimp fabrics. *Compos A* 102: 322-335, 2017.
- [15] Dörr D, Henning F, Kärger L: Nonlinear hyperviscoelastic modelling of intra-ply deformation behaviour in finite element forming simulation of continuously fibre-reinforced thermoplastics. *Comp A* 109:585-596, 2018.
- [16] Hamila N, Boisse P, Chatel S. Semi-discrete shell finite elements for textile composite forming simulation. *Int J Mat Form*, 2(1):169–172, 2009.
- [17] Boisse P, Colmars J, Hamila N, Naouar N, Steer Q. Bending and wrinkling of composite fiber preforms and prepregs. A review and new developments in the draping simulations. *Compos B*: 141:234–249, 2018.
- [18] d'Agostino MV, Giorgio I, Greco L, Madeo A, Boisse P. Continuum and discrete models for structures including (quasi-) inextensible elasticae with a view to the design and modeling of composite reinforcements. *Int. J. Solids & Structures* 59:1–17, 2015.
- [19] Khan MA, Mabrouki T, Vidal-Sallé E, Boisse P. Numerical and experimental analyses of woven composite reinforcement forming using a hypoelastic behaviour. Application to the double dome benchmark. *Journal of Materials Processing Technology*, 210(2):378–388, 2010.
- [20] Machado M, Fischlschweiger M, Major Z. A rate-dependent non-orthogonal constitutive model for describing shear behaviour of woven reinforced thermoplastic composites. *Compos A* 80:194–203, 2016.
- [21] Lin H, Long AC, Sherburn M, Clifford MJ. Modelling of mechanical behaviour for woven fabrics under combined loading. *Int J Mat Forming* 1(1):899–902, 2008.
- [22] Nosrat Nezami F, Gereke T, Cherif C. Analyses of interaction mechanisms during forming of multilayer carbon woven fabrics for composite applications. *Compos A* 84:406–416, 2016.
- [23] Lomov SV, Ivanov D, Verpoest I, Zako M, Kurashi T, Nakai H, Hiroswawa S. Meso-FE modelling of textile composites: Road map, data flow and algorithms. *Compos Sci Techn* 67(9):1870–1891, 2007.
- [24] Sirtautas J, Pickett AK, Lépicier P. A mesoscopic model for coupled drape-infusion simulation of biaxial non-crimp fabric. *Compos B*, 47:48–57, 2013.
- [25] Böhler P, Härtel F, Middendorf P. Identification of Forming Limits for Unidirectional Carbon Textiles in Reality and Mesoscopic Simulation. *Key Engineering Materials* 554-557:423–32, 2013.
- [26] Schirmaier FJ, Weidenmann KA, Kärger L, Henning F: Characterisation of the draping behaviour of unidirectional non-crimp fabrics (UD-NCF). *Compos A* 80: 28–38, 2016.
- [27] Haanappel S. Forming of UD fibre reinforced thermoplastics: A critical evaluation of intra-ply shear. Phd thesis, Universität Enschede, 2013.
- [28] Cao J, Akkerman R, Boisse P, Chen J, Cheng HS et al. Characterization of mechanical behavior of woven fabrics - Experimental methods and benchmark results. *Compos A* 39: 1037-1053, 2008.
- [29] ten Thije R, Akkerman R, Huétink J. Large deformation simulation of anisotropic material using an updated lagrangian finite element method. *Comp Meth Appl Mechanics & Engineering*, 196(33-34):3141–3150, 2007.
- [30] Galkin J, Kunze E, Kärger L, Böhm R, Gude M: Experimental and numerical determination of the local fiber volume content of unidirectional non-crimp fabrics with forming effects. *J Compos Sci* 3, 19, 2019.
- [31] Kunze E, Galkin J, Röger B, Böhm R, Kärger L, Gude M: Experimental Description of Draping Effects and their Influence on the Structural Behavior of Fiber Reinforced Composites. ICCM 22, Melbourne, 2019.
- [32] Guzman-Maldonado E, Hamila N, Naouar N, Moulin G, Boisse P. Simulation of thermoplastic prepreg thermoforming based on a visco-hyperelastic model and a thermal homogenization. *Mater Des* 93:431–42, 2016.
- [33] Dörr D, Joppich T, Kugele D, Henning F, Kärger L: A coupled thermomechanical approach for finite element forming simulation of continuously fiber-reinforced semi-crystalline thermoplastics. *Compos A* 125: 105508, 2019.
- [34] Spencer A. Theory of fabric-reinforced viscous fluids. *Composites Part A: Applied Science and Manufacturing*, 31(12):1311-1321, 2000.
- [35] Ziabicki A, *Fundamentals of Fibre Formation: The Science of Fibre Spinning and Drawing*, John Wiley & Sons, Ltd, 1976.
- [36] Kugele D, Dörr D, Wittemann F, Hangs B, Rausch J, Kärger L, Henning F. Modelling of the Non-Isothermal Crystallization Kinetics of Polyamide 6 Composites During Thermoforming. *AIP Conf Proc* 1896,030005, 2017.
- [37] Kugele D, Rausch J, Müller P, Kärger L, Henning F, Temperature Distribution in Thickness Direction of Thermoplastic Laminates During Thermoforming, *Proc Int Conf Automotive Compos*, Portugal, 2016.
- [38] Dörr D. Simulation of the thermoforming process of UD fiber-reinforced thermoplastic tape laminates, Doctoral thesis, Karlsruhe Institute of Technology (KIT), 2019.
- [39] Bergmann J, Dörmann H, Lange R. Interpreting process data of wet pressing process. Part 1 & Part 2, *J Comp Mat* 50 (17): 2399–2407 & 2409–2419, 2016.
- [40] Poppe C, Dörr D, Henning F, Kärger L. A 2D modeling approach for fluid propagation during FE-forming simulation of continuously reinforced composites in wet compression moulding. *AIP Conf Proc* 1960, 020022, 2018.
- [41] Poppe C, Dörr D, Henning F, Kärger L: Experimental and numerical investigation of the shear behaviour of infiltrated woven fabrics, *Compos A* 114: 327-337, 2018.
- [42] Poppe C, Rosenkranz T, Dörr D, Kärger L. Comparative experimental and numerical analysis of bending behaviour of dry and low viscous infiltrated woven fabrics, *Compos A* 124: 105466, 2019.
- [43] Poppe C, Dörr D, Henning F, Kärger L. Experimental and numerical investigation of the contact behavior during FE forming simulation of continuously reinforced composites in wet compression molding, *AIP Conf Proc* 2113, 020002, 2019.
- [44] Poppe C, Albrecht F, Krauß C, Kärger L. A 3D Modelling Approach for Fluid Progression during Process Simulation of Wet Compression Moulding – Motivation & Approach, *Proc Manuf.*, accepted, 2020.
- [45] Schäfer B, Dörr D, Kärger L. Reduced-Integration 8-Node Hexahedral Solid-Shell Element for the Macroscopic Forming Simulation of Continuous Fibre-Reinforced Polymers, *Proc Manuf.*, accepted, 2020.